Real-Time Observation of Local Strain Effects on Nonvolatile Ferroelectric Memory Storage Mechanisms

Christopher R. Winkler,[†] Michael L. Jablonski,[†] Khalid Ashraf,[‡] Anoop R. Damodaran,[§] Karthik Jambunathan,[§] James L. Hart,[†] Jianguo G. Wen,[∥] Dean J. Miller,[∥] Lane W. Martin,[§] Sayeef Salahuddin,[‡] and Mitra L. Taheri*,[†]

[†]Department of Materials Science & Engineering, Drexel University, Philadelphia, Pennsylvania 19104, United States

[‡]Department of Electrical Engineering and Computer Sciences, University of California, Berkeley, California 94720, United States

[§]Department of Materials Science & Engineering and Materials Research Laboratory, University of Illinois, Urbana−Champaign, Illinois 61801, United States

[∥]Electron Microscopy Center, Argonne National Laboratory, Argonne, Illinois 60439, United States

S *Supporting Information*

ABSTRACT: We use in situ transmission electron microscopy to directly observe, at high temporal and spatial resolution, the interaction of ferroelectric domains and dislocation networks within $BiFeO_3$ thin films. The experimental observations are compared with a phase field model constructed to simulate the dynamics of domains in the presence of dislocations and their resulting strain fields. We demonstrate that a global network of misfit dislocations at the film−substrate interface can act as nucleation sites and slow down domain propagation in the vicinity of the dislocations. Networks of individual threading dislocations emanating from the film−electrode interface play a more dramatic role in pinning domain motion. These dislocations may be responsible for the domain behavior in ferroelectric thin-film devices deviating from conventional Kolmogorov−Avrami−Ishibashi dynamics toward a Nucleation Limited Switching model.

KEYWORDS: *In situ TEM, ferroelectric domain switching, multiferroic, strain*
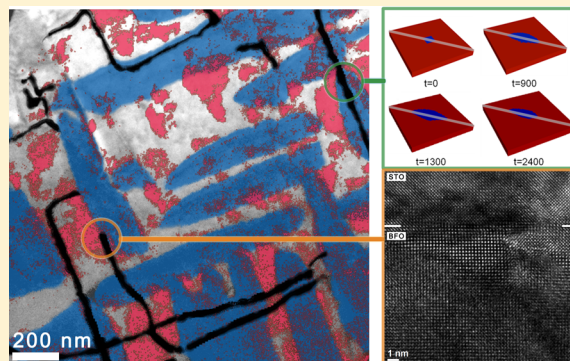
Electric-field tuning of magnetism via exchange bias coupling permits construction of a range of sensors and tunable devices made of magnetoelectric materials such as $BiFeO_3$.[1−4] Experimental demonstration of direct electric field induced tuning of magnetism has been achieved using multiferroic heterostructures,[1,4−7] but the behavior of magnetization was found to be critically controlled by the dynamics of ferroelectric domains of $BiFeO_3$. As a result, one of the outstanding challenges in the realization of room temperature magnetoelectric memory devices today is the need to develop a better understanding of ferroelectric domain dynamics in nanostructured multiferroic films. Traditionally, two main models have been used for ferroelectric switching: the Kolmogorov−Avrami−Ishibashi (KAI) and the Nucleation Limited Switching (NLS) models.[8,9] In nanoscale device geometries, ferroelectric switching behavior can deviate from the widely accepted KAI model, possibly due to microstructural defect and interface density.[8,9] Point defects, dislocations, and other domain walls can all act as pinning centers for domain motion.[10−16] Both theoretical and experimental studies have shown that strain fields around threading dislocations result in ~1 nm "dead" areas (near-zero polarization), which pin domain

walls.[10,16,17] Variations in Burger's vectors of misfit or threading dislocations have also been shown to alter local domain morphology and nucleation behavior.[12] While the KAI model is typically used to describe domain switching in bulk and microscale ferroelectrics, the NLS model has been found to better fit thin-film devices and nanoscale capacitors.[19] The NLS model treats ferroelectric switching as nucleation-limited, in which the ratio of nucleation sites (i.e., defects and domain walls) to nuclei per unit volume increases with shrinking device geometries. Three factors that control device performance must be explored experimentally: (1) switching speed of ferroelectric domains, (2) ferroelectric domain size and density, and (3) the stability of the domains. A crucial limiting factor during switching is that the elastic interactions can affect stability of switched domains, which can lead to an erasing of nonvolatile information storage.[20,21]

Domain wall mobility and morphology are directly impacted by their surrounding environment (i.e., local microstructure and chemistry).[22] In ferroelectric materials, dislocations can
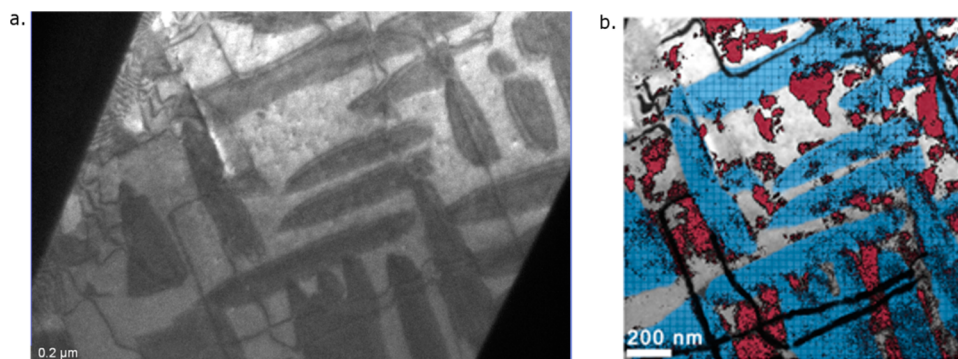
Figure 1. Plan view TEM images of the domain morphology and constructed nucleation map. A selected frame taken from an in situ video showing the initial conditions before biasing (a) and the postanalysis nucleation map (b). In panel b, the original location of the domains is shown in blue with internal cross-hatching; newly formed domains during biasing are highlighted in red; and fixed threading dislocations are emphasized in black. The applied field was ~210 V/cm.
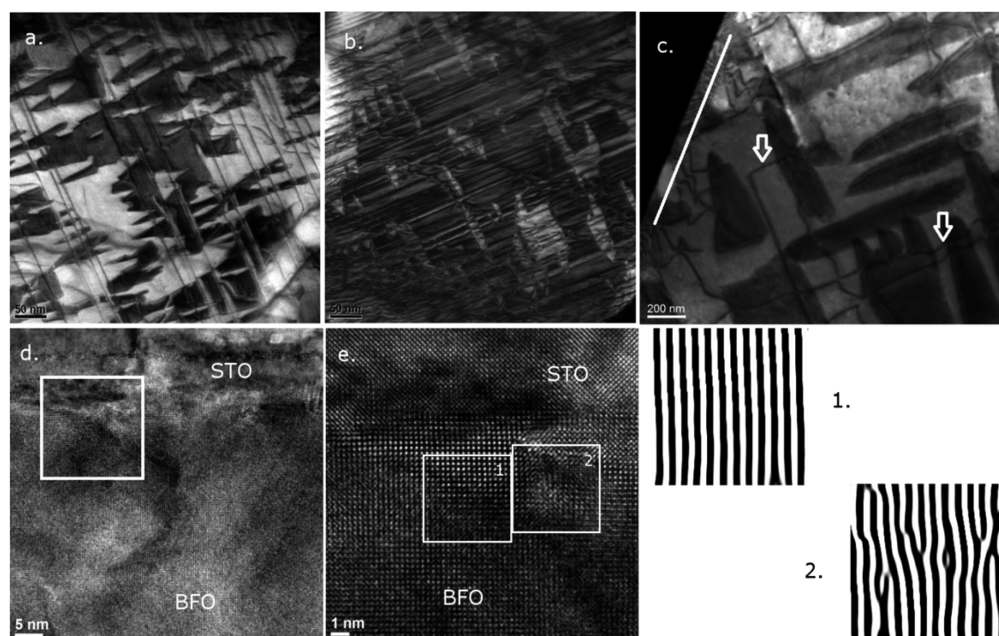

Figure 2. Plan view and cross section images of $BiFeO_3$ devices on $SrTiO_3$ substrates. The orthogonal network of misfit dislocations can be seen in panels a and b with the corresponding diffraction vectors indicated. Several threading dislocations emanating from the electrode edge (white line) are indicated by arrows in panel c. High-resolution images of cross sections in panels d and e reveal the presence of a dislocation at the interface of the $BiFeO_3$ and $SrTiO_3$ at a suspected 71° domain wall. Inverse fast Fourier transforms formed using the (100) reflections reveal pristine lattice planes across the domain wall (1) with an edge dislocation (2) near the $BiFeO_3/SrTiO_3$ interface. These results show that dislocations tend to cluster along domain walls in strained $BiFeO_3$ films.

cause domain wall pinning and local changes in polarization stability.[10−14,18] To fully understand domain stability in the presence of defects (found in devices), ferroelectric switching should be analyzed in an environment and geometry that mimics that of the device. Various techniques have been employed to study ferroelectric domain dynamics at the nanoscale,[7,14,17,23−33] including recent efforts using transmission electron microscopy (TEM).[17,26−28] In many of these studies,[27,28] a localized applied bias was used, similar to that utilized in piezoresponse force microscopy. While such experiments provide insight into highly localized domain behavior, they failed to show global domain−domain interactions due to limitations of the localized probe. Moreover, while defect−domain and domain−domain interactions were discussed, the role of defects and strain in domain evolution was not elucidated.

In this letter, through the use of in situ and high-resolution, aberration-corrected TEM coupled with phase field modeling, we find that local domain kinetics can deviate from the KAI model locally; globally, however, the KAI model is an accurate model of domain kinetics. Specifically, we investigate the contribution of strain fields resulting from the formation of dislocations to produce a quantitative description of domain behavior and stability. Our correlative approach to the study of domain evolution in electric fields provides a direct, quantitative measurement of the role of localized strain components (tensile and compressive) in ferroelectric switching. The work presented herein provides insight into the switching behavior of devices containing significant defect densities and directly shows the interactions between dislocations and domain walls, revealing a preference for domain nucleation to locally follow the NLS model over the
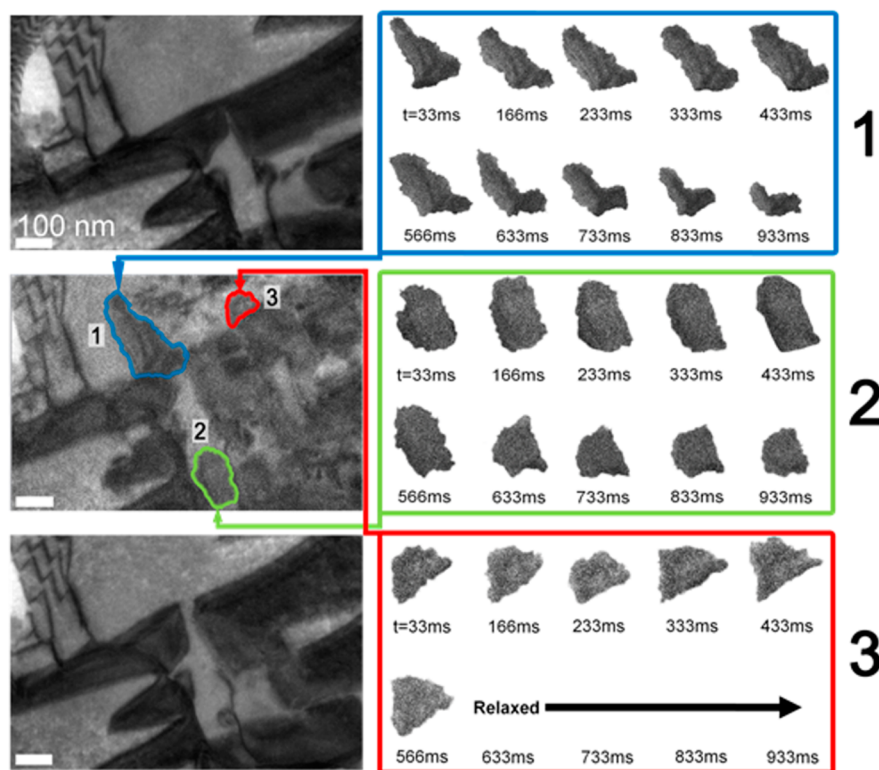
Figure 3. Morphological evolution of three transient domain structures formed during biasing. The environment around each of the three domains is materially different: domain 1 is relatively unhindered and free to propagate under the influence of the applied field; domain 2 is bordered on either side by threading dislocations; and domain 3 is constrained by neighboring domains. Each TEM image uses the same length of scale bar. Highlighted morphologies of the three domains are not to scale.

KAI model, while the global behavior follows the KAI model.[17] The results prove that the direct impact of strain and defects is a crucial factor for determining the appropriate switching mechanism for ferroelectric domains in nanoscale device architectures.

Our experimental approach, described in refs 17 and 26 enables real-time monitoring of an entire device structure during in situ operation at length scales capable of probing one-dimensional defects (dislocations) and their interaction with moving ferroelectric domain walls. As described in the Supporting Information, the films used were grown with in-plane electrodes, which eliminate the sample surface−probe tip barrier present in experiments using scanning probes to initiate ferroelectric switching and thus the presence of asymmetric electronic boundary conditions, which give rise to internal biases in the material that impact switching dynamics. The large field of view permits the simultaneous observation of all ferroelectric domains within the volume of a device as well as the real-time interaction of domains with other domains and dislocations under bias. Real-time imaging of the ferroelectric device under bias (plan view) enables the construction of nucleation maps covering large areas that reveal the exact location of newly formed domains, the quantification of the density and sites of domain nucleation, and the isolation of test cases for quantifying how domain wall propagation and relaxation velocities are affected by the presence of the dislocations in the as-grown device assembly. By comparing a set of images extracted from in situ video, before, during, and after a few hundred milliseconds after the initiation of a voltage pulse, the changes in the domain structures due to nucleation and propagation are isolated. These nucleation maps serve as a

visualization of the global domain nucleation behavior at a glance (Figure 1). The prebias domain configuration and area analyzed are depicted in Figure 1a, and the nucleation map is shown in Figure 1b. Nucleation events are observed predominantly at the existing domain walls. The domains nucleate along existing walls, which run along both the [100] and [010]. The nucleated domains, however, are driven primarily along the [010] direction under the applied electric field.

While it is known that the NLS model takes domain−domain interactions into account, the direct effect of dislocations and their strain fields needs to be addressed to fully understand the deviation of domain switching from the KAI model. The strain fields associated with both the threading and misfit dislocations present in the sample depicted in Figure 1 contribute heavily to the overall nucleation and switching behavior of the thin-film structure. Plan view TEM imaging reveals a network of misfit dislocations at the interface between the film and substrate and a network of threading dislocations at the film−electrode interface (Figure 2). These misfit dislocations form as a result of the growth conditions to accommodate for the lattice mismatch between the $BiFeO_3$ films and $SrTiO_3$ substrate. As the epitaxial film has a larger lattice parameter (pseudocubic, 3.96 Å) versus the substrate (3.905 Å), the film is under compression and forms misfit dislocations in order to accommodate the strain. Both domains and misfit dislocation networks are clearly visible by orienting the electron beam to excite sets of {110} using low index reflections. The density of dislocations in the orthogonal network (Figures 2a,b) with Burger's vectors $\mathbf{b} = [100]$ is ~1.8 × 10^9 cm^{-2} and for dislocations with $\mathbf{b} = [010]$ is ~2.0 × 10^9 cm^{-2}. The density of
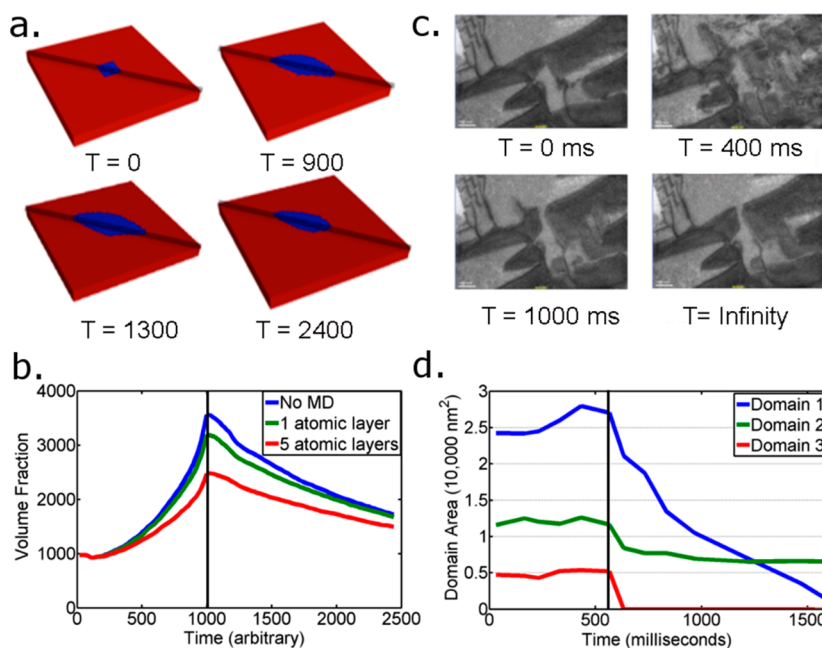
Figure 4. Comparison of simulated and experimental results with plotted domain areas. Left: The dynamic behavior of the domains as a function of strain due to misfit dislocation. An electric field was applied from 100 to 1000 time steps. (a) Color plot of a nucleated domain on the single atomic layer misfit dislocation. The domain initially grows along the misfit dislocation (up to 1000 time steps) and then relaxes as the applied field is removed (up to 2450 time steps here). (b) Both the domain growth rate under the applied field and domain relaxation are slower as single atomic layer misfit dislocation is introduced. Introduction of an artificial 5 layer misfit dislocation reduces the domain wall velocity further confirming the trend that increased compressive misfit dislocation reduces the domain growth and relaxation when the domain is growing along the misfit dislocation. (c) Experimental images extracted from the in situ video showing the nucleation and growth of domains near a network of threading dislocations (dark lines). Each image in the sequence is of the same scale. (d) Domain areas plotted over time for the domains highlighted in Figure 3. Domains near threading dislocations tend to be pinned, while nucleation occurs more often near the dislocation network.

such dislocations dictates that every domain visible in Figure 1 crosses at least one misfit dislocation and that the domains contain at least one misfit dislocation running parallel to the long axis. Cross-sectional analysis of the films using aberration-corrected TEM reveals that domain walls are entangled with dislocations and point defect clusters. Figure 2d shows a 71° domain wall with a defect structure near the film/substrate interface. HRTEM of this area reveals one large defect present at this domain wall (Figure 2e). Inverse fast Fourier transforms (IFFTs) formed using the (100) and (−100) reflections inside the boxed regions reveal an edge-type dislocation at the intersection of the domain and the $SrTiO_3$ substrate, which can add electrostatic potential and potentially lead to domain nucleation or pinning.[34]

On the basis of the microstructure shown in Figures 1 and 2, three unique behaviors are analyzed by outlining and tracking three domains using frames from the in situ videos captured under an applied bias of ~115 V/cm (Figure 3). These domains are chosen as test cases to provide a comparison for the evolution of the morphologies of each of these domains versus time, highlighting differences related to the microstructural environment surrounding the domains. Domain 1 is primarily unhindered by other domains in the as-grown configuration (however, newly nucleated domains do interact with domain 1 during biasing). Domain 2 is bordered on the left and right sides by threading dislocations. Domain 3 is in an environment similar to that of Domain 1, with the addition of other domains in close proximity. A voltage was applied for ~600 ms and then switched off, allowing the domains to relax. Domain 1, relatively unhindered, expanded in area over the entire ~600 ms during which the voltage was applied. Other

nucleated domains visible to the right of domain 1 do hinder its expansion, or increase of lateral domain size, resulting in an asymmetric domain shape. Domains 2 and 3, both of which were corralled by neighboring domains or defects, remained constant over time until ~600 ms. Immediately after 600 ms, as the bias is turned off, domains 1 and 3 began to reverse their direction of propagation and relax. Domain 3 fully relaxed before domain 1 due to its smaller size and domain−domain repulsion. While the size of the relaxed domain is linked to the rate of relaxation, it is not the sole contributing factor. Domains 1 and 3 fully relaxed at different times, but at a roughly equivalent rate. Domain 2, however, relaxed at a dramatically slower rate, continuing to shrink well after the field was removed, due to its proximity to two threading dislocations. The threading dislocations adjacent to and pinning domain 2 originated from this dislocation network. Because this domain dislocation network can support the nucleation of new domains and retard the dynamics of those nucleated domains,[15] it can have a strong effect on the polarization dynamics of these devices.

By exploring the role of compressive versus tensile misfit dislocation networks further through phase field simulation,[35] we have shown that the strain from a compressive dislocation can retard the forward and relaxation velocity of domains within the vicinity of the dislocation. Domain nucleation can also be enhanced by these dislocations. To initiate domain propagation in a manner representative of the experiments, a lateral electric field (200 kV/cm) was applied along the $BiFeO_3$ [110] crystal direction, and a nucleated domain (blue) was introduced at a compressive misfit dislocation along the [010] direction (black line in Figure 4a). This domain grew and

propagated under the influence of the applied field and then relaxed when the field was turned off. From these simulations, images were created showing the lateral expansion of a single domain along a misfit dislocation (Figure 4a), which were then used to plot the projected domain area versus time (Figure 4b). Three different configurations were simulated. First, without the presence of a dislocation, the domain growth and relaxation were the fastest. In the experimental data, domain 1 corresponds to this type of domain growth. The introduction of a compressive dislocation was found to slow both the domain growth and relaxation rates as shown in Figure 4b. Increasing the number of atomic layers of the compressive dislocation further reduced the growth and relaxation velocities of domains along the dislocation, consistent with our experimental observation of domain 2, which clearly grew along the threading dislocation in Figure 2b. The opposite effect was observed for simulated tensile misfit dislocations in that the domain growth and relaxation velocity increased along these dislocations.

The simulation results reveal that compressively strained dislocations with [010] Burger's vector act to reduce domain wall velocity along the length of the dislocation. Increasing the compressive strain around the dislocation was found to further decrease the domain velocities near these dislocations. Compressive dislocations with [100] Burger's vectors were revealed to act as nucleation sites, allowing newly forming domains to nucleate ahead of existing propagating domains. The reduction of domain wall switching energy in the vicinity of this type of dislocation enables it to act as a nucleation site, which is consistent with Figure 1b. For comparison, frames were extracted from in situ video examined with the corresponding changes in domain areas from Figure 3 plotted over time (Figures 4c,d). Figure 4c shows the domain morphologies over time in the presence of the network of dislocations near the electrode edge and near several visible threading dislocations. The domain areas from Figure 3 are plotted in Figure 4d for comparison to the modeling results with domains near threading dislocations that exhibit compressive strains acting as pinning or stabilizing sites as predicted by the model. Under the influence of the applied field, the existing propagating domains and those nucleating at the dislocation coalesce, which is consistent with experimental observations.

The modeled and experimentally observed domain dynamics indicate that the presence of dislocations impacts domain kinetics, and most importantly, the strain relationship of these dislocations to the thin film in the device appears to be the controlling factor in domain nucleation, growth, and relaxation. The misfit dislocation network, though it shows different densities along the two orthogonal directions, is a global defect network. All parts of the $BiFeO_3$ thin film between the electrodes show very similar misfit dislocation networks. As shown in the phase field model presented, the network of tensile misfit dislocations do not directly affect the domain wall velocity under applied bias. Intersections of the misfit dislocations have been observed to act globally as nucleation sites during the domain switching process. Threading dislocations, especially the network formed at the electrode–film interface, are not uniformly distributed through the volume of the $BiFeO_3$ film. Because of the threading dislocations being present in the bulk of the film and thus contributing both a tensile and compressive strain to the surrounding film, the predicted domain wall behavior due to compressive strain can

occur. The density of threading dislocations can thus strongly affect domain kinetics, as parts of the $BiFeO_3$ film with many threading dislocations will show different domain kinetics than others with a lower concentration of these defects. Such an influence is clearly observed in the experimental in situ videos and provides an explanation as to why deviations from the KAI model can occur.

Our experiments show that while domain switching generally, or globally, follows the KAI model, interactions between single domains and single dislocations can locally alter the behavior and kinetics of domain switching. The experimental nucleation maps, however, show that domain nucleation occurs simultaneously, within the temporal resolution of the technique, at domain walls. The compartmentalized model of nucleation described by the NLS model does not agree with the experimental evidence, as domain nucleation is observed globally at existing domain walls. While enhanced nucleation of domains was observed at defects and along domain walls providing favorable energetic states as predicted by the NLS model, the overall switching behavior more closely follows the KAI model. Separating the sample into elementary units can be used to determine where nucleation will occur; however, the global behavior observed in these experiments further validates the KAI model as dominating domain wall motion.

We demonstrate that the ability to observe domain propagation and relaxation at time and length scales that reveal fundamental domain behavior using our in situ biasing experiments. The results are comparable with those produced by piezoresponse force microscopy, yet the temporal resolution of this in situ technique permits study of the intermediate behaviors involved in ferroelectric switching. Moreover, the range of spatial resolutions available in the TEM and the sensitivity of the technique to defects and dislocations enables the capturing of domain–defect and domain–domain interactions, an advantage over piezoresponse force microscopy. The influence of certain types of compressive dislocations is shown to impact the domain kinetics of ferroelectric domain switching. These compressive dislocations, due to their effect on domain nucleation and domain velocities combined with their bunched distribution through the volume of the film, may explain why these $BiFeO_3$ devices exhibit local kinetics, which deviates from the expected KAI model. Globally, however, the experimentally observed nucleation and propagation behaviors support the KAI model of domain kinetics. Domain–defect interactions are found to be highly local, limited to single domain and single dislocation interactions, while most switching and nucleation is observed to occur globally and within concurrent timeframes. The combined temporal and spatial dynamics thus show that domain behavior can be very different at the nanoscale and macroscale; by capturing both scales simultaneously, we are able to provide a unique view to how mesoscopic domain behavior form from microscopic dynamics.

■ ASSOCIATED CONTENT

ⓢ Supporting Information
Experimental methods. This material is available free of charge via the Internet at http://pubs.acs.org.

■ AUTHOR INFORMATION

Corresponding Author
*(M.L.T.) E-mail: mtaheri@coe.drexel.edu.

■ REFERENCES

(1) Lee, D.; Yang, S. M.; Kim, T. H.; Jeon, B. C.; Kim, Y. S.; Yoon, J.-G.; Lee, H. N.; Baek, S. H.; Eom, C. B.; Noh, T. W. *Adv. Mater.* **2011**, 402−406.

(2) Bibes, M.; Barthélémy, A. *Nat. Mater.* **2008**, *7*, 425−426.

(3) Chu, Y.; Martin, L. W.; Holcomb, M. B.; Ramesh, R.; Division, M. S.; Berkeley, L. *Mater. Today* **2007**, *10*, 16−23.

(4) Seidel, J.; Martin, L. W.; He, Q.; Zhan, Q.; Chu, Y.-H.; Rother, A.; Hawkridge, M. E.; Maksymovych, P.; Yu, P.; Gajek, M.; Balke, N.; Kalinin, S. V.; Gemming, S.; Wang, F.; Catalan, G.; Scott, J. F.; Spaldin, N. A.; Orenstein, J.; Ramesh, R. *Nat. Mater.* **2009**, *8*, 229−234.

(5) Pantel, D.; Goetze, S.; Hesse, D.; Alexe, M. *Nat. Mater.* **2012**, *11*, 2−11.

(6) Evans, D. M.; Schilling, A.; Kumar, A.; Sanchez, D.; Ortega, N.; Arredondo, M.; Katiyar, R. S.; Gregg, J. M.; Scott, J. F. *Nat. Commun.* **2013**, *4*, 1534.

(7) Gruverman, A.; Rodriguez, B. *Appl. Phys.* **2005**, *87*, 082902.

(8) Kim, Y.; Han, H.; Lee, W.; Baik, S.; Hesse, D.; Alexe, M. *Nano Lett.* **2010**, *10*, 1266−1270.

(9) Pantel, D.; Chu, Y.-H.; Martin, L. W.; Ramesh, R.; Hesse, D.; Alexe, M. *J. Appl. Phys.* **2010**, *107*, 084111.

(10) Alpay, S. P.; Misirlioglu, I. B.; Nagarajan, V.; Ramesh, R. *Appl. Phys. Lett.* **2004**, *85*, 2044.

(11) Li, Y. L.; Hu, S. Y.; Choudhury, S.; Baskes, M. I.; Saxena, A.; Lookman, T.; Jia, Q. X.; Schlom, D. G.; Chen, L. Q. *J. Appl. Phys.* **2008**, *104*, 104110.

(12) Hu, S. Y.; Li, Y. L.; Chen, L. Q. *J. Appl. Phys.* **2003**, *94*, 2542.

(13) Gao, P.; Nelson, C. T.; Jokisaari, J. R.; Baek, S.-H.; Bark, C. W.; Zhang, Y.; Wang, E.; Schlom, D. G.; Eom, C.-B.; Pan, X. *Nat. Commun.* **2011**, *2*, 591.

(14) Kalinin, S. V.; Rodriguez, B. J.; Borisevich, A. Y.; Baddorf, A. P.; Balke, N.; Chang, H. J.; Chen, L.-Q.; Choudhury, S.; Jesse, S.; Maksymovych, P.; Nikiforov, M. P.; Pennycook, S. J. *Adv. Mater.* **2010**, *22*, 314−322.

(15) Dawber, M.; Rabe, K.; Scott, J. *Rev. Mod. Phys.* **2005**, *77*, 1083.

(16) Misirlioglu, I. B.; Alpay, S. P.; Aindow, M.; Nagarajan, V. *Appl. Phys. Lett.* **2006**, *88*, 102906.

(17) Winkler, C. R.; Jablonski, M. L.; Damodaran, A. R.; Jambunathan, K.; Martin, L. W.; Taheri, M. L. *J. Appl. Phys.* **2012**, *112*, 052013.

(18) Vrejoiu, I.; Rhun, G.; Le; Zakharov, N. *Philos. Mag.* **2006**, *28*, 4477−4486.

(19) Tagantsev, A.; Stolichnov, I.; Setter, N. *Phys. Rev. B* **2002**, 1−6.

(20) Baek, S. H.; Jang, H. W.; Folkman, C. M.; Li, Y. L.; Winchester, B.; Zhang, J. X.; He, Q.; Chu, Y. H.; Nelson, C. T.; Rzchowski, M. S.; Pan, X. Q.; Ramesh, R.; Chen, L. Q.; Eom, C. B. *Nat. Mater.* **2010**, *9*, 309−314.

(21) Zhao, T.; Scholl, A.; Zavaliche, F.; Lee, K.; Barry, M.; Doran, A.; Cruz, M. P.; Chu, Y. H.; Ederer, C.; Spaldin, N. A.; Das, R. R.; Kim, D. M.; Baek, S. H.; Eom, C. B.; Ramesh, R. *Nat. Mater.* **2006**, *5*, 823−829.

(22) Lee, K.; Baik, S. *Annu. Rev. Mater. Res.* **2006**, *36*, 81−116.

(23) Martin, L. W.; Chu, Y.-H.; Ramesh, R. *Mater. Sci. Eng., R* **2010**, *68*, 89−133.

(24) Balke, N.; Bdikin, I.; Kalinin, S. V.; Kholkin, A. L. *J. Am. Ceram. Soc.* **2009**, *92*, 1629−1647.

(25) Kim, D.; Jo, J.; Kim, T.; Yang, S. *Appl. Phys.* **2007**, *91*, 132903.

(26) Winkler, C. R.; Damodaran, A. R.; Karthik, J.; Martin, L. W.; Taheri, M. L. *Micron* **2012**, *43*, 1121−1126.

(27) Nelson, C. T.; Gao, P.; Jokisaari, J. R.; Heikes, C.; Adamo, C.; Melville, A.; Baek, S.; Folkman, C. M.; Winchester, B.; Gu, Y.; Liu, Y.; Zhang, K.; Wang, E.; Li, J.; Chen, L. *Science* **2011**, *2643*, 968−971.

(28) Chang, H.; Kalinin, S.; Yang, S. *J. Appl.* **2011**, *110*, 052014.

(29) Hruszkewycz, S. O.; Folkman, C. M.; Highland, M. J.; Holt, M. V.; Baek, S. H.; Streiffer, S. K.; Baldo, P.; Eom, C. B.; Fuoss, P. H. *Appl. Phys. Lett.* **2011**, *99*, 232903.

(30) Do, D.-H.; Evans, P. G.; Isaacs, E. D.; Kim, D. M.; Eom, C. B.; Dufresne, E. M. *Nat. Mater.* **2004**, *3*, 365−369.

(31) Scholl, A. *Curr. Opin. Solid State Mater. Sci.* **2003**, *7*, 59−66.

(32) Vogel, J.; Kuch, W.; Bonfim, M.; Camarero, J.; Pennec, Y.; Offi, F.; Fukumoto, K.; Kirschner, J.; Fontaine, A.; Pizzini, S. *Appl. Phys. Lett.* **2003**, *82*, 2299.

(33) Chen, Y.-C.; He, Q.; Chu, F.-N.; Huang, Y.-C.; Chen, J.-W.; Liang, W.-I.; Vasudevan, R. K.; Nagarajan, V.; Arenholz, E.; Kalinin, S. V.; Chu, Y.-H. *Adv. Mater.* **2012**, *24*, 3070−3075.

(34) Wang, Y.; Nelson, C.; Melville, A.; Winchester, B.; Shang, S.; Liu, Z.-K.; Schlom, D. G.; Pan, X.; Chen, L.-Q. *Phys. Rev. Lett.* **2013**, *110*, 267601.

(35) Ashraf, K.; Salahuddin, S. *J. Appl. Phys.* **2012**, *112*, 074102.